Proc. World Haptics 2007, pp. 403-408, Tsukuba (Japan), Mar., 2007.

Free-Form Tactile Sensor Using 3-Dimensional Shape Capture Sheet

Takayuki Hoshi and Hiroyuki Shinoda
The University of Tokyo
{star, shino}@alab.t.u-tokyo.ac.jp

Abstract

We are developing a novel sensing device named "3-dimensional capture sheet (3DCS)". The cloth-like sheet measures its own 3D configuration. The sheet enables us to make a soft tactile sensor by wrapping a compressible material in it. The number, shapes, and positions of objects are obtained from the surface deformation of the material. The contact forces are also estimated. There is a lattice structure inside the sheet, and each link of the structure has a triaxial accelerometer. The roll and pitch angles of the link are derived from the gravity vector measured by the accelerometer. Furthermore, the relative yaw angle is also determined owing to the lattice structure. The posture of each link is fully described by these three angles. Then, the whole shape of the sheet is estimated by combining all of the links in computation.

1. Introduction

Measurement of the 3D shape of an object is usually conducted by the optical methods (e.g. stereo vision, structured light projection, shape from focus/defocus and so on). They need external equipments and suffer from the occlusion problem.

We propose another shape measurement approach, in which a cloth-like sensing device named "3-dimensional capture sheet (3DCS)" is used. The sheet has the ability to acquire its own 3D configuration, and measures the shape of an object by wrapping it directly. This method needs only the foldable sheet and no other external equipments. With the sheet, you can measure the shape and size of an object with ease. The human posture can also be measured by the sheet worn.

The sheet also can be utilized as a soft tactile sensor. Softness is one of the most important factors for tactile sensor skins on robots [1]. The tactile sensor is a compressible material, such as urethane foam, wrapped by the sheet. The number, shapes, and positions of contact objects are obtained because the whole surface profile of the material is observed by the sheet. The contact forces are also estimated from the surface deformation and Young's modulus of the material. The structure of the tactile sensor is so simple that it enables us to attach it to a free-form surface of a robot, or make a stuffed toy which has tactile, haptic, and somatic sensation.

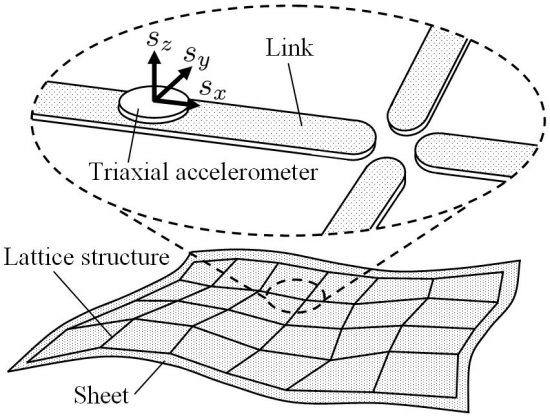

Figure 1. Structure of 3DCS.

The 3DCS, the key component of the proposed tactile sensor, is the sheet in which there is a lattice structure (Fig. 1). A triaxial accelerometer is attached on each link, and measures the gravity vector. The posture of the link is estimated from the measured gravity. The gravity measurement has been used in motion capture in the preceding reports [2, 3]. They use the gravity to derive only the roll and pitch angles of a human arm because the output of a single triaxial accelerometer contains only the information about the two angles. They use other types of sensors such as an electromagnetic compass or a gyro sensor to know the yaw angle. Unlike them, we use multi accelerometers and thereby estimate also the yaw angles without any other sensors. The 3D configuration of the sheet can be

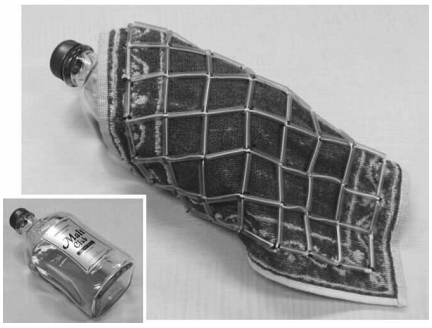

Figure 2. 7×7 lattice model made of 2.5-cm tubes combined with strings.

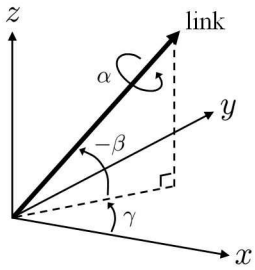

Figure 3. Definition of rotational angles.

measured without being affected by any electric or magnetic noises because the sensing theory of the sheet is based on the gravity. Besides, the theory is based on geometry without temporal operation. Therefore the measurement is less subject to the offset of the sensor output than the temporal integration method.

This device is motivated by the recent trend of MEMS and sensor networking technologies that enable us to implant a large number of low-cost miniaturized sensors in elastic cloth-like materials [4]. The rest of this paper is organized as follows. Firstly, Section II describes the basic structure and the theory of 3D shape reconstruction of the 3DCS. Next, the feasibility of the sheet is examined by simulation in Section III. Then, the prototype is presented in Section IV. Finally, we conclude this paper in Section V.

2. Three-dimensional capture sheet

2.1. Structure

The illustration of the 3DCS is shown in Fig. 1. There is a lattice structure inside of it, and each link of the structure has a triaxial accelerometer. The accelerometers measure the gravity vector, and the measured data are sent to the host computer. The x-axis of the triaxial accelerometer is aligned along the link direction, and the z-axis is aligned along the direction

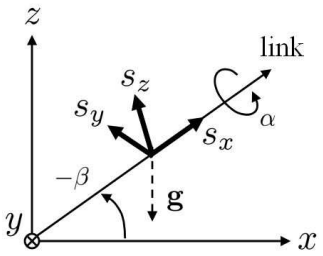

Figure 4. Side view. The sensor coordinate is rotated according to *α* and *β*.

of the normal vector on the sheet. The all link lengths are the same. The stretching property of the lattice structure is anisotropic as is the case with a textile cloth, i.e. it is stretchable only along the diagonal directions). Assuming a smooth curved shape, we can cover its surface with the structure. Fig. 2 shows the lattice model made of tubes combined with strings for demonstration.

2.2. Sensing theory

In the "shape from gravity" theory, we firstly introduce the following assumption.

[Assumption 1]
The acceleration by motion of the link is negligible compared with the gravity acceleration.

Then the shape estimation in dynamic motion is out of consideration at least in this stage. The posture of each link is described by three angles based on the world coordinate; roll α [rad], pitch β [rad], and yaw γ [rad] (Fig. 3). Whereas only the roll and pitch angles are derived from the measured sensor data, the relative yaw angle is determined owing to the lattice structure. After the angles of the all links are obtained, the whole shape of the 3DCS is estimated by combining the links in a computational 3D space. Note that the estimated shape still has the uncertainty of orientation in the world coordinate.

The angles of the link are obtained as follows. Here we assume that each axis of the triaxial accelerometer is aligned along the corresponding axis of the world coordinate (i.e. the x-axis of the accelerometer to the x-axis of the world coordinate) at the initial condition.

2.1.1. Roll and pitch angles. These angles are derived directly from the gravity vector measured by the accelerometer on each link. The rotation matrix $\mathbf{G}_{\beta\alpha}$, from the world coordinate to the sensor coordinate (Fig. 4), is described as

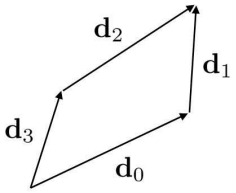

Figure 5. Assumption 2, about directional vectors.

$$\mathbf{G}_{\beta\alpha} \equiv \begin{bmatrix} \cos\beta & 0 & \sin\beta \\ 0 & 1 & 0 \\ -\sin\beta & 0 & \cos\beta \end{bmatrix} \begin{bmatrix} 1 & 0 & 0 \\ 0 & \cos\alpha & -\sin\alpha \\ 0 & \sin\alpha & \cos\alpha \end{bmatrix} = \begin{bmatrix} \cos\beta & \sin\beta\sin\alpha & \sin\beta\cos\alpha \\ 0 & \cos\alpha & -\sin\alpha \\ -\sin\beta & \cos\beta\sin\alpha & \cos\beta\cos\alpha \end{bmatrix}. \quad (1)$$

Each column of $\mathbf{G}_{\beta\alpha}$ means the axes of the sensor coordinate direction in the world coordinate after rotated, and hence the output vector of the accelerometer $\mathbf{s}=[s_x, s_y, s_z]^{\mathrm{T}}$ is represented as a product of the transposed matrix of $\mathbf{G}_{\beta\alpha}$ and the gravity vector $\mathbf{g}=[0, 0, -g]^{\mathrm{T}}$ (where g [m/s^2] is the gravity acceleration);

$$\mathbf{s} = \mathbf{G}_{\beta\alpha}^{\mathrm{T}}\mathbf{g} = \begin{bmatrix} g\sin\beta \\ -g\cos\beta\sin\alpha \\ -g\cos\beta\cos\alpha \end{bmatrix}. \quad (2)$$

Then we can derive α and β by solving (2).

2.1.2. Yaw angles. This angle cannot be derived from the output of the single accelerometer. Then we take note of one unit of the lattice structure composed of four links forming a quadrangle to derive the yaw angles, making two assumptions.

The first assumption is about the directional vector $\mathbf{d}_i$ (i is the link identification) which is represented as

$$\mathbf{d}_i \equiv \begin{bmatrix} \cos\gamma_i & -\sin\gamma_i & 0 \\ \sin\gamma_i & \cos\gamma_i & 0 \\ 0 & 0 & 1 \end{bmatrix} \mathbf{G}_{\beta_i\alpha_i} \begin{bmatrix} 1 \\ 0 \\ 0 \end{bmatrix} = \begin{bmatrix} \cos\gamma_i\cos\beta_i \\ \sin\gamma_i\cos\beta_i \\ -\sin\beta_i \end{bmatrix}. \quad (3)$$

Because the lattice unit is a closed loop (Fig. 5), "the two routes reach the same point in the 3D space." That results in the assumption of the link rigidness as

[Assumption 2]

$$\mathbf{d}_0 + \mathbf{d}_1 = \mathbf{d}_3 + \mathbf{d}_2. \quad (4)$$

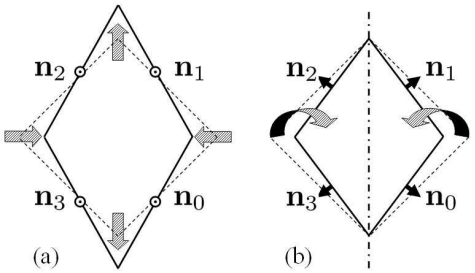

Figure 6. Assumption 3, about normal vectors. Symmetric transformations, (a) squashing and (b) folding.

The other assumption is about the normal vector $\mathbf{n}_i$ which is represented as

$$\mathbf{n}_i \equiv \begin{bmatrix} \cos\gamma_i & -\sin\gamma_i & 0 \\ \sin\gamma_i & \cos\gamma_i & 0 \\ 0 & 0 & 1 \end{bmatrix} \mathbf{G}_{\beta_i\alpha_i} \begin{bmatrix} 0 \\ 0 \\ 1 \end{bmatrix} = \begin{bmatrix} \cos\gamma_i\sin\beta_i\cos\alpha_i + \sin\gamma_i\sin\alpha_i \\ \sin\gamma_i\sin\beta_i\cos\alpha_i - \cos\gamma_i\sin\alpha_i \\ \cos\beta_i\cos\alpha_i \end{bmatrix}. \quad (5)$$

We assume the 3DCS is mounted on a smooth curved shape, and the lattice unit transforms in symmetric manners (Fig. 6). In other words, "one average of the normal vectors of an opposed link pair must be equal to the other," that is

[Assumption 3]

$$\mathbf{n}_0 + \mathbf{n}_2 = \mathbf{n}_1 + \mathbf{n}_3. \quad (6)$$

We can get γ_i by solving (4) and (6). Note that at least one of γ_i should be fixed at a certain value preliminarily to determine the four parameters γ_i in principle. In other words, all we can do is to determine the relative yaw angels of γ_1, γ_2 and γ_3 to γ_0.

Estimating the configuration of the multi-unit lattice structure is straightforward. After the same algorithm is applied to each lattice unit, the whole configuration is estimated by combining the estimated unit shapes.

2.3. Unsolvability analysis

The unsolvable conditions of (4) and (6) are clarified by the singular value decomposition [5]. Now (4) and (6) are rewritten as a matrix form, that is,

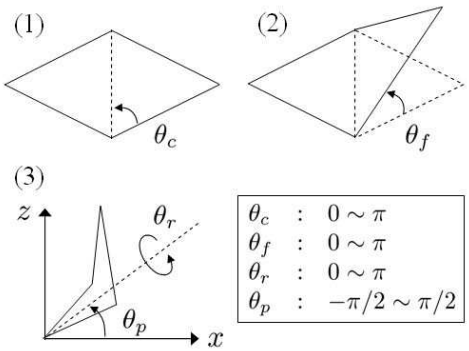

Figure 7. Procedure of lattice model generation.

$$\begin{bmatrix} -c\beta_1 & 0 & c\beta_2 & 0 & c\beta_3 & 0 \\ 0 & -c\beta_1 & 0 & c\beta_2 & 0 & c\beta_3 \\ s\beta_1\, c\alpha_1 & s\alpha_1 & -s\beta_2\, c\alpha_2 & -s\alpha_2 & s\beta_3\, c\alpha_3 & s\alpha_3 \\ -s\alpha_1 & s\beta_1\, c\alpha_1 & s\alpha_2 & -s\beta_2\, c\alpha_2 & -s\alpha_3 & s\beta_3\, c\alpha_3 \end{bmatrix} \begin{bmatrix} c\gamma_1 \\ s\gamma_1 \\ c\gamma_2 \\ s\gamma_2 \\ c\gamma_3 \\ s\gamma_3 \end{bmatrix} = \begin{bmatrix} c\gamma_0\, c\beta_0 \\ s\gamma_0\, c\beta_0 \\ c\gamma_0\, s\beta_0\, c\alpha_0 + s\gamma_0\, s\alpha_0 \\ s\gamma_0\, s\beta_0\, c\alpha_0 - c\gamma_0\, s\alpha_0 \end{bmatrix} \quad (7)$$

where "s" and "c" stand for "sin" and "cos", respectively. The z-components of (4) and (6) are excluded because they do not contain any γ_i. Here γ_0 is a fixed number to be the root of the orientation, and the other γ_i (i=1, 2, 3) are obtained as relative values to γ_0. If the 4×6 coefficient matrix has less than three nonzero singular values, (7) is underdetermined and the configuration of the lattice unit cannot be estimated uniquely.

The state of the lattice unit is characterized by four angle parameters; corner θ_c [rad], fold θ_f [rad], roll θ_r [rad], and pitch θ_p [rad] (Fig. 7). In the following calculation, we quantize each angle is divided into 20 discrete values at even intervals. Fig. 8 reveals the unsolvable situations of (θ_c, θ_f, θ_r, θ_p). The points plotted in Fig. 8 stand for the conditions on which the ratio of the third singular value λ_3 to the first largest singular value λ_1 is less than 0.1 (i.e. λ_3/λ_1<0.1).

From Fig. 8, it turns out that all the unsolvable conditions are roughly included in the following two cases:

[Case 1] The all links of the lattice unit are laid on a horizontal plane, i.e. (θ_f, θ_r, θ_p)=(0, 0, 0), (0, π, 0), (π, 0, 0), or (π, π, 0).
[Case 2] The lattice unit is fully squashed, i.e. θ_c=0, π, or θ_f=π.

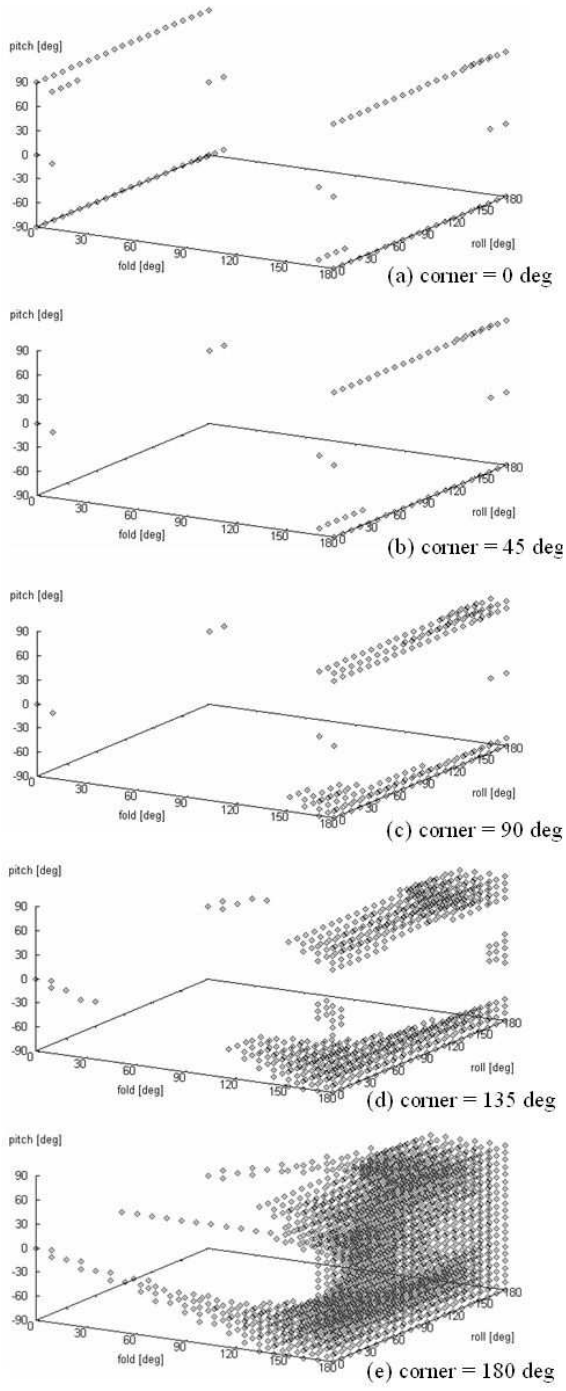

Figure 8. Results of unsolvability analysis. The (θ_c, θ_f, θ_r, θ_p)s satisfying λ_3/λ_1<0.1are plotted in the parameter space.

Note that Case 2 is avoidable by setting limits to the link joints in real devices. As a result, the possible unsolvable condition is Case 1, the horizontal case.

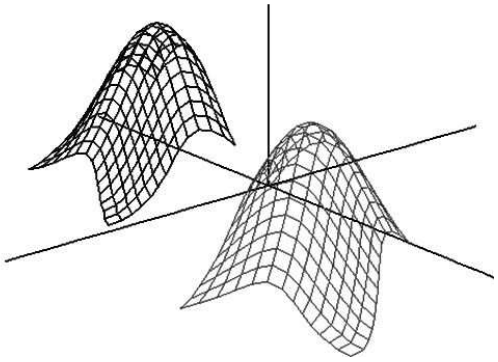

Figure 9. Simulation result. The far and near plots are the model and estimated shapes, respectively.

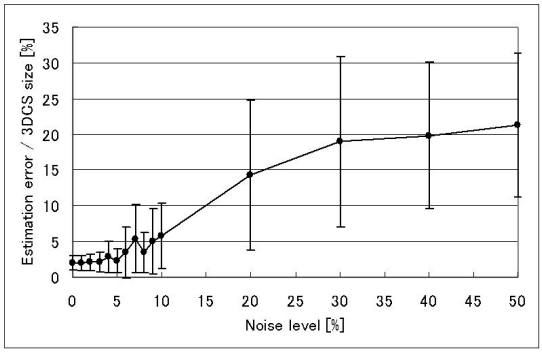

Figure 10. Simulation results on effect of noise. The mean values (dots) and the standard deviations (error bars) of the estimation error.

3. Simulations and results

3.1. Methods

In the data acquisition process, we firstly design a 13×13 spring-mass model of the 3DCS. In the model, the link is modeled as a very hard spring so that the link length does not change, and the joint as a mass. After the model is laid over a target shape by iterative calculation, the direction of the sensor axes are simulated, and then the sensor outputs are calculated.

In the shape estimation process, the roll and pitch angles are derived analytically from (2). Because it is hard to derive the yaw angles analytically from (4) and (6), the following numerical calculation is conducted. Firstly, we modify (4) and (6) into a minimization problem, that is

$$P \equiv \sum_{j\in\{x,y,z\}} \{(d_{0j} + d_{1j} - d_{2j} - d_{3j})^2 + (n_{0j} - n_{1j} + n_{2j} - n_{3j})^2\} \to \min. \quad (8)$$

where j is the coordinate identification. Now, α_i and β_i are given. If the minimum value of P is equal to zero, the solution for (8) are also the solution for (4) and (6). Secondly, we solve (8) by the steepest descent method. Although (8) has several local minimums, we can overcome them by trying multiple initial values.

3.2. Shape estimation result

Firstly, we show an example of general situations using a Gaussian as a target shape. Fig. 9 shows the model shape and the estimated shape. The Gaussian shape is successfully reproduced.

3.3. Effect of noise on sensor data

The previous result (Fig. 9) is obtained without noise. The possible causes of disturbance are the noise on the sensor data (i.e. angle error), the change of the link length, and the violation of the normal vector assumption (6). Since the major factor seems the noise on the sensor data, the simulation investigates the stability of the 3DCS under various S/N ratios of the accelerometers. The noise is generated using the Mersenne Twister algorithm [6] and added to each component of the sensor data. Here, the noise level is represented as the percentage of the noise compared to the gravity g.

Fig. 10 shows the mean values and the standard deviations of the estimation errors, the distances between the corresponding joints of the model and estimated shapes. The distances are calculated after overlapping the estimated shape to the model shape by the least-squares method to match their orientations and positions. 1,960 samples (196 joints × 10 trials) are used in statistical calculation. According to our observation, the estimation seems to fail discernibly when the estimation error goes beyond 5 % of the side length of the 3DCS. Then, Fig. 10 suggests that the 3DCS decently works with the noise level up to 5 % (i.e. about 0.5 m/s^2 in acceleration). We think that the accuracy is practically achievable.

4. Prototype of lattice unit

4.1. System Specifications

The developed prototype is one lattice unit (Fig. 11). It consists of four acrylic links (20 cm in length) and four triaxial accelerometers (5×5 mm^2) mounted on

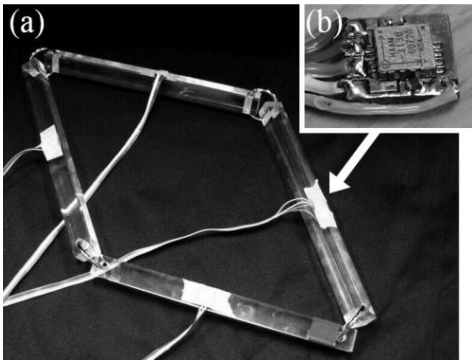

Figure 11. (a) Prototype of one lattice unit. (b) The triaxial accelerometer.

small substrates (1×1 cm^2). The links are jointed by metal rings.

The PC imports the analog sensor readouts via 50-Hz-cutoff LPFs and 12-bit A/D converters. The effective sampling rate of the system is 145 Hz. Here, the conjugate gradient method [5] is applied in the estimation process for real-time performance.

4.2. Demonstration

Fig. 12 shows the demonstration of the shape estimation of the one-unit prototype. The shape of the prototype is successfully estimated in real time.

The quantitative evaluation of the prototype is conducted. With the shape of the prototype set to certain angle parameters, $(\theta_c, \theta_f, \theta_r, \theta_p)=(\pi/6, 3\pi/10, \pi, 3\pi/10)$, the coordinate values of the estimated joint positions are recorded. The mean value and the standard deviation of the estimation errors is 11.3 % and 0.8 % of the link length (i.e. about 2.2 cm and 1.6 mm in length for the 20-cm link), respectively. This estimation error is due to the alignment error of the accelerometer, the characteristics of the joint, the computational error in the estimation process, and the noise in the analog signal lines.

5. Conclusion

A new tactile sensor is proposed in this paper. The sensor is based on the sheet which measures its own 3-dimensional configuration using distributed triaxial accelerometers. The structure and sensing theory of the sheet are described. The theory clarifies that the proposed estimation method works well outside the trivial cases. A one-unit prototype is developed and the 3D shape estimation is demonstrated with 11.3 % estimation error.

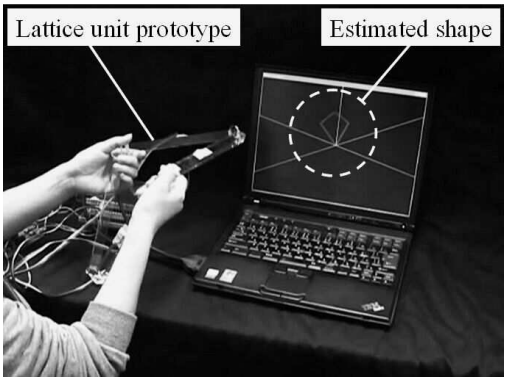

Fig. 12. Demonstration of shape estimation.

After examining and improving the accuracy of the prototype, in the next stage, we will develop the small-sized sensor chip on which an LSI is mounted with the triaxial accelerometer. The LSI measures the sensor readouts by A/D converters and sends digital data to the host computer via the two-dimensional communication sheet [4]. Then the practical 3DCS is realized without complicated, long, and/or analog-signal wires. The proposed tactile sensor is developed as one application of the sheet.

References

[1] M. H. Lee and H. R. Nicholls, "Tactile sensing for mechatronics - a state of the art survey," *Mechatronics*, vol. 9, pp. 1-31, 1999.

[2] J. Lee and I. Ha, "Real-time motion capture for a human body using accelerometers, *Robotica*, vol. 19, pp. 601-610, 2001.

[3] N. Miller, O. C. Jenkins, M. Kallmann, and M. J. Mataric, "Motion capture from inertial sensing for untethered humanoid teleoperation, *Proc. 4th IEEE/RAS International Conference on Humanoid Robots (Humanoids 2004)*, vol. 2, pp. 547-565, 2004.

[4] Y. Makino, H. Chigusa and H. Shinoda, "Two-dimensional sensor integration using resonant proximity connector –Basic technology and application to elastic interface device–," *Proc. 3rd International Conference on Networked Sensing Systems (INSS 2006)*, pp. 196-202, 2006.

[5] W. H. Press, S. A. Teukolsky, W. T. Vetterling, and B. P. Flannery, *Numerical Recipes in C: The Art of Scientific Computing Second Edition*, Cambridge University Press, 1992.

[6] M. Matsumoto and T. Nishimura, "Mersenne Twister: A 623-dimensionally equidistributed uniform pseudorandom number generator," *ACM Trans. on Modeling and Computer Simulation*, vol. 8, no. 1, pp.3-30, 1998.